Journal of Energy Storage 32 (2020) 101893

Contents lists available at ScienceDirect

Journal of Energy Storage

journal homepage: www.elsevier.com/locate/est

Thermal management analysis using heat pipe in the high current discharging of lithium-ion battery in electric vehicles

Hamidreza Behi[a,b,*], Danial Karimi[a,b], Mohammadreza Behi[c,d], Joris Jaguemont[a,b], Morteza Ghanbarpour[d], Masud Behnia[e], Maitane Berecibar[a,b], Joeri Van Mierlo[a,b]

[a] Research group MOBI – Mobility, Logistics, and Automotive Technology Research Centre, Vrije Universiteit Brussel, Pleinlaan 2, Brussels 1050, Belgium
[b] Flanders Make, Heverlee 3001, Belgium
[c] The University of Sydney, School of Chemical and Biomolecular Engineering, NSW 2006, Australia
[d] Department of Energy Technology, KTH Royal Institute of Technology, SE-10044 Stockholm, Sweden
[e] Macquarie Business School, Macquarie University, Sydney, Australia

ARTICLE INFO

Keywords:
Lithium-ion (Li-ion) battery
Thermal management system (TMS)
Heat pipe
Liquid cooling system embedded heat pipe (LCHP)
Computational fluid dynamic (CFD)

ABSTRACT

Thermal management system (TMS) for commonly used lithium-ion (Li-ion) batteries is an essential requirement in electric vehicle operation due to the excessive heat generation of these batteries during fast charging/discharging. In the current study, a thermal model of lithium-titanate (LTO) cell and three cooling strategies comprising natural air cooling, forced fluid cooling, and a flat heat pipe-assisted method is proposed experimentally. A new thermal analysis of the single battery cell is conducted to identify the most critical zone of the cell in terms of heat generation. This analysis allowed us to maximize heat dissipation with only one heat pipe mounted on the vital region. For further evaluation of the proposed strategies, a computational fluid dynamic (CFD) model is built in COMSOL Multiphysics® and validated with surface temperature profile along the heat pipe and cell. For real applications, a numerical optimization computation is also conducted in the module level to investigate the cooling capacity of the liquid cooling system and liquid cooling system embedded heat pipe (LCHP). The results show that the single heat pipe provided up to 29.1% of the required cooling load in the 8C discharging rate. Moreover, in the module level, the liquid cooling system and LCHP show better performance compared with natural air cooling while reducing the module temperature by 29.9% and 32.6%, respectively.

1. Introduction

In recent decades, lithium-ion (Li-ion) batteries have gained popularity as a significant power source for different applications including electric and hybrid vehicles, power grids, and solar energy storage. Owing to high power density, reliability, and durability, Li-ion batteries are highly recommended as a power source in a long driving range and fast acceleration [1,2]. Nonetheless, Li-ion batteries produce heat throughout fast charge and discharge cycles at a high current level. Besides, their energy storage capacity and longevity are highly dependent on temperature and inhomogeneity [3,4]. Several studies showed that the high temperature of the Li-ion battery cells accelerates capacity degradation and shortens battery life [5–8]. Heat accumulation in batteries also leads to safety issues and abnormality in the entire system of electric vehicles. Overheating, burning, and the explosion of batteries are some of these safety risks. Thus, the design and development of an effective thermal management system (TMS) remain a crucial challenge in the electric vehicles industry [9,10]. The optimum operating temperature range for Li-ion batteries is between 25–40 °C [11,12]. This temperature range within the Li-ion battery results in a balance between performance and lifetime [13]. In order to reach a higher speed, acceleration, and lower charging time of the battery pack, fast charging/discharging mods have imposed an urgent challenge on battery power performance, and the battery TMS. By far, several cooling systems in the form of active, passive, and hybrid are examined to meet the heat dissipation requirement of Li-ion batteries. Phase change material (PCM) and nanomaterials, heat pipe, air, and liquid cooling systems are used as TMS to control the heat generation of the electronic devices [14–17] and batteries during operation [18–27]. For this aim PCM, air, and water have been used as a coolant.

Among the mentioned cooling systems, heat pipes are highly under the attention because of high heat transfer efficiency, low cost and

* Corresponding author at: Research group MOBI – Mobility, Logistics, and Automotive Technology Research Centre, Vrije Universiteit Brussel, Pleinlaan 2, Brussels 1050, Belgium.

E-mail address: hamidreza.behi@vub.ac.be (H. Behi).

https://doi.org/10.1016/j.est.2020.101893
Received 24 April 2020; Received in revised form 17 September 2020; Accepted 18 September 2020

Nomenclature

Δt	Time Interval (t)
T	Battery Temperature (K)
I	Discharge Current (Ah)
V	Operating Voltage (V)
v	Velocity (m/s)
m	Operating Voltage (V)
c_p	Specific Heat capacity (J/kg.K)
T_{amb}	Temperature of ambient (K)
R_{bt}	Total Resistance of the Battery Tab (K/W)
R_{tab}	Total Resistance of the Battery (K/W)
k	Thermal Conductivity (W/m.K)
p	Pressure (Pa)
ρ'	Resistivity (K/W)
S	Cross-section of the Tab and Cell (m^2)
h	Heat Transfer Coefficient (W/m^2.K)
q_{conv}	Free Cooling Heat Transfer (W)
Q_{Cell}	Power Loss of Battery (W)
g_i	Gravity (m/s^2)
u	Air velocity (m/s)
L_{eff}	Effective Transport Length of the Heat Pipe (m)
L_a	Adiabatic Length of Heat Pipe (m)
L_c	Condenser Length of Heat Pipe (m)
L_e	Evaporator Length of Heat Pipe (m)
k_{eff}	Effective Thermal Conductivity of the Heat Pipe (W/m.K)
Q_{hp}	Heat Transferred by Heat pipe (W)
A_h	The cross-section of the Heat pipe (m^2)
q_g	Cell Heat Generation (W)
V	Volume (m3)
D	Total Drag Force
F	Friction Drag
k	Turbulent Kinetic Energy
s	Second

Greek

$\forall$	Volume of Battery Cell (m^2 /s)
μ	Dynamic Viscosity (Pa.s)
ρ	Density (kg/m^3)
λ	Heat Generation
ε	Energy Dissipation Rate
μ_t	Turbulent Viscosity

Acronyms

CFD	Computational Fluid Dynamics
TMS	Thermal Management System
LCHP	Liquid Cooling Embedded with Heat Pipe
HP	Heat Pipe
SOC	State of Charge
Li-ion	Lithium-ion
PCM	Phase Change Material

maintenance, lightweight, and high lifetime. The heat pipe is a passive cooling system with a simple structure and working fluid transport. They can be used in many cooling applications and particularly electric vehicles [15,28–32]. Researchers have investigated the heat pipe assisted cooling systems for battery packs because of their advantages– high heat dissipation efficiency– over inefficient air convection subjected to high-heat flux, or bulky liquid cooling driven by pumps, and low thermal conductivity of PCMs [33–37]. In brief, the heat pipe thermal conductivity is almost 90 times higher compared with a copper bar in the same dimension [38]. Dan et al. [39] employed a micro-heat pip array in designing a thermal management system for 96 prismatic batteries. They found that the temperature stability under fast-changing operating conditions is achievable to a great extent by using the micro heat pipe array. Behi et al. [40] numerically considered the effect of the L shaped heat pipe on maximum temperature and temperature uniformity of a cylindrical battery module. Rao et al. [41] designed a heat pipe TMS for the prismatic cells. They kept the temperature of cells within the preferred range under unstable operating and cycling test conditions. Feng et al. [42] fabricated a heat pipe cooling device to reduce the operating temperature and strain. They found that the strain and temperature decreased after using the heat pipe in a charge-discharge cycle process. Wang et al. [33] recommended a heat pipe TMS for cooling and heating purposes. They found if the heat generation is less than 10 W/cell, the system can control the battery temperature in the optimum temperature range. Most of the thermal management system are focusing on the low C rates(1.5C [40]; 0.5C-1C [42]; 1C-3C [39]; 1C-4C [33]). The C rate indicates the speed of charging/discharging of the cell respect to its maximum capacity. For example, in the 1C rate current, the entire capacity of a cell will be discharged in one hour. In the same way for the fast charging/discharging, the battery cell is required to be charged/discharged at a high C rate in 10 minutes [43]. It is necessary to mention that as the C rate goes higher the heat generation of the cell increases as well. Therefore, the existing TMSs are probably not able to control the severe scenarios in high current applications. Moreover, most TMSs suffer from temperature inhomogeneity in the battery pack. Therefore they need to use a bulky cooling system or many heat pipes to control the temperature of the module/pack [44–48]. Hence, engineering of an efficient TMS with the least number of heat pipes and a higher safety margin to control the temperature in battery modules/packs is necessary for the EV industry.

In order to design an efficient TMS, a comprehensive thermal analysis and applied design strategies are required. To the authors' knowledge, the thermal analysis of Li-ion cells in high current discharging to identify the critical zone in terms of heat generation has been rarely addressed in the literature. Due to the lack of thermal analysis, a huge cooling system embedded with many heat pipes is used to control the temperature of the module/pack. The current study focuses on the thermal performance improvement of heat pipe based TMS. Firstly, a multizone analysis of the battery cell and identifying the zone with the highest heat generation, given the non-uniform cell temperature/heat generation distribution. This multizone analysis, using thermal imaging, contributed to a smarter design to achieve acceptable cooling performance with the least number of heat pipes in the high current application. The charging /discharging current rate of the LTO cell is recommended by the factory by a minimum of 4.6 A to a maximum of 92 A. However, in the current case, the temperature distribution of the cell is studied at the 8 C discharging rate (184 A). According to the temperature recording and thermal camera pictures, the non-uniform heat generation and temperature inhomogeneity are

Table 1
The main properties of the heat pipe.

Parameter	Value
Heat pipe length (mm)	250
Dimension L × W (mm)	11.2 × 3.5
Working fluid	Distilled water
Wick structure	Sintered
Thermal conductivity (W/m.K)	8212
Cooling Power (W)	100
Operation temperature (°C)	30–120
Cross-section area (mm^2)	38.32
L_{eff}(mm)	125

Table 2
The main properties of the cell.

Parameter	Value
Chemistry	LTO
Shape	Prismatic
Nominal Voltage (V)	2.3
Maximum voltage (V)	2.7
Minimum voltage (V)	1.5
Capacity (Ah)	23
Specific Energy (J/kg)	96
Energy Density (J/m)	202
Weight (kg)	0.550
Volume (L)	0.260
Dimensions L × W × H (mm)	115 × 22 × 103
Heat specific capacity (J/kg.K)	1150
Thermal conductivity x,y,z (W/m.K)	31, 0.8, 31

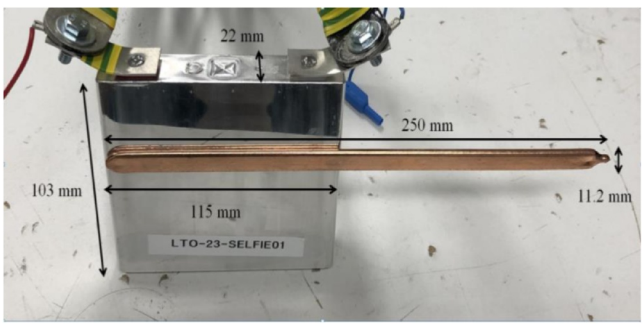

Fig. 1. The LTO prismatic cell and heat pipe with their dimensions.

Table 3
The uncertainties of the experimental parameters.

Parameter	Uncertainty
Current (A)	± 0.1%
Voltage (V)	± 0.1%
Thermocouple (°C)	± 0.2
Data logger (°C)	± 0.025

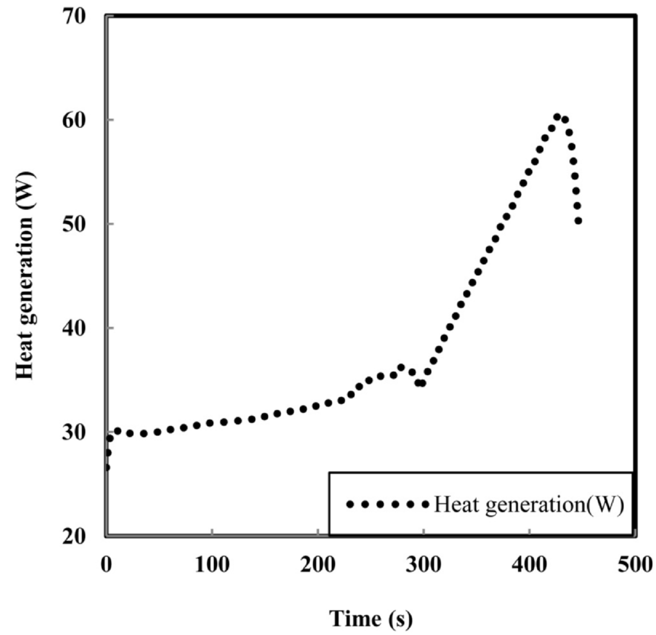

Fig. 3. The heat generation of cell in 8C discharging rate.

identified inside the cell [49]. The most critical region is revealed in the center and top of the cell with the highest heat generation rate. Based on this thermal analysis, it is shown that a single heat pipe placed in the most critical zone is sufficient for the cooling and cell operation under the desired condition. Furthermore, for more investigation, a module consisting of 15 cells numerically simulated and optimized by a liquid cooling system and LCHP during the 8 C discharging rate. The results demonstrated acceptable performance of the engineered cooling system while minimizing the weight and volume of the module in real applications.

2. Experimental setup

2.1. Description of the battery and flat heat pipe

The experimental setup was built to investigate the performance of the heat pipe for the cooling of the LTO battery cell. The selection of a proper heat pipe is an essential item in designing a cooling system. Cylindrical heat pipes are broadly used in the past decades in many research and industrial applications for their efficient cooling [50–52]. However, the ability to connect on the surface of the heat source is a crucial item. Therefore, a flat heat pipe from DigiKey was made of copper has been selected [53]. For the working fluid in the same configuration, a water heat pipe probably have a lower thermal resistance compared with a methanol heat pipe [44]. Moreover, it has a suitable range of operation temperature for the thermal management of the battery. Thus distilled water working fluid has been selected. The sintered copper is chosen as a wick structure because it is less affected by the gravity and heat source orientation compared with the other kind of

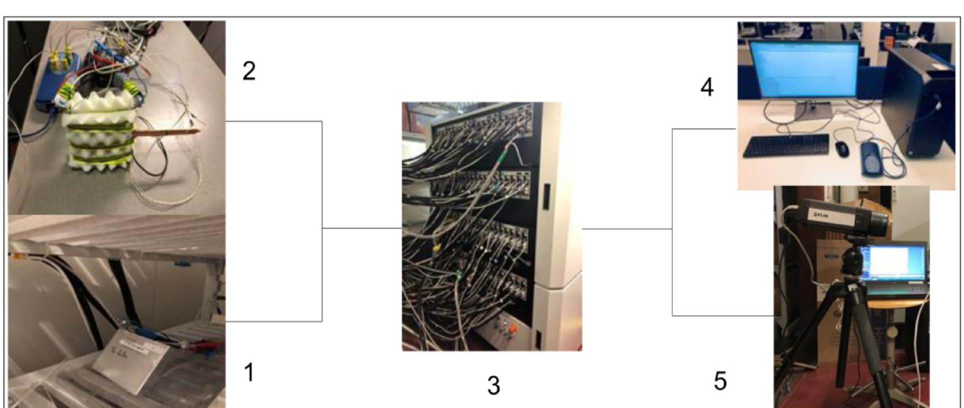

Fig. 2. The picture of the experimental system. (1) prismatic cell; (2) isolated prismatic cell and heat pipe; (3) PEC® battery tester (4) personal computer and data logger; (5) thermal Camera.

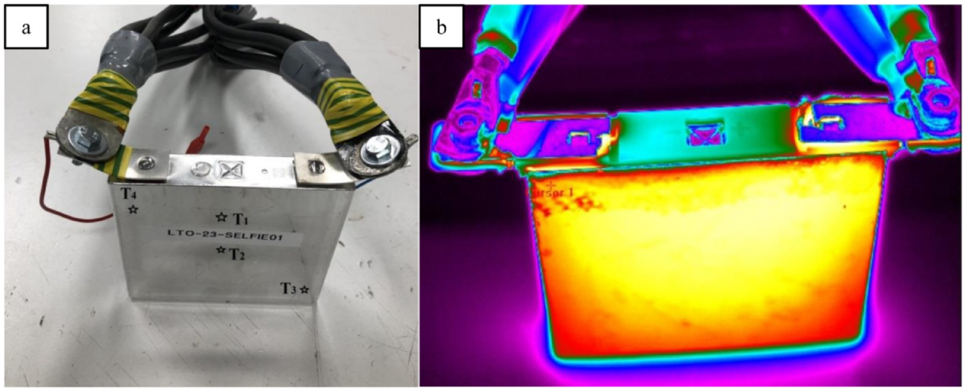

Fig. 4. The picture of the experimental test (a) and location of thermocouples in the presence of natural air cooling and (b) its infrared picture at the end of the 8 C discharging rate test (446s).

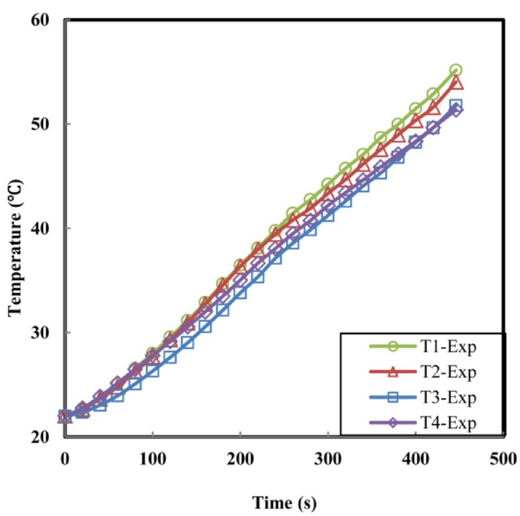

Fig. 5. The temperature variation of the LTO cell in natural air cooling at an initial temperature of 22 °C (Exp: Experimental).

wicks [54,55]. Table 1 presents the main parameters of the flat heat pipe. The LTO 23 Ah cell has been chosen for the tests. The main features of the prismatic LTO cell are presented in Table 2, whereas Fig. 1 shows the picture of the cell and heat pipe with their dimensions.

2.2. Description of the test setup

In the current study, the performance of natural air cooling and forced air cooling embedded with flat heat pipe has been investigated on the LTO prismatic Li-ion cell. The picture of the test setup is shown in Fig. 2. The experimental setup included a PEC battery tester, a cooling fan, a flat heat pipe, a prismatic cell, a Pico USB TC-08 data logger, twelve K-type thermocouples, a thermal camera, and a personal computer. The thermocouples with the accuracy of ± 0.2 °C are connected to the cell and heat pipe.

In order to start the cycling, the battery tester connected to the cell, and a personal computer connected to the data logger to record the temperatures. The voltage and current of the cell are being monitored during cycling. The discharging of the cell is done using the testers in which the cell is discharged by the current rate of 8 C (184 A) at 446 s. After connecting the cell to the data logger, and connecting the voltage and current cables, the cell will be charged/discharged. By charging/discharging the cell, voltage, and current, as well as the resistance of the battery, are characterized. The heat generation of the cell can be calculated as follows:

$$q_g = R_{bt} \cdot I^2 = V \cdot I \tag{1}$$

where V and I represent the voltage and the current respectively [56].

To calculate the uncertainty, the Schultz and Cole [57,58] method have been used.

$$U_R = \left[\sum_{i=1}^{n} \left(\frac{\partial R}{\partial V_I} U_{VI} \right)^2 \right]^{1/2} \tag{2}$$

where U_{VI} and U_R are the error of each factor and total errors respectively. Table 3 shows the measurement correctness of each factor. The maximum uncertainty is less than 2.01%.

2.3. Experimental results and discussion

2.3.1. Natural air cooling

Considering the effect of natural air cooling on the cell is the initial phase to investigate thermal performance. Fig. 3 shows the generated heat inside the battery cell in the 8 C discharge rate. The average of the heat generation is 37.65 W which is calculated based on Eq. (1). Fig. 4 is taken by a thermal camera and shows the temperature distribution of the cell in a natural air cooling strategy while the ambient temperature is 22 °C at the end of the discharging process (446 s).

As it is evident in the temperature distribution of the cell, there is a hot zone in the middle and top of the cell.

The natural air cooling test was done comprising of discharging the cell with a high constant current of 184 A from 100% to 0% of the state of charge (SOC) and at an initial temperature of 22 °C. The thermocouples of T_1-T_4 are shown in Fig. 4a that measures the temperature of the cell. The temperature difference of the tests is calculated by subtracting the current battery temperature with the initial battery temperature. Fig. 5 shows the temperature variation of the LTO cell in natural air cooling. The temperatures of thermocouples T_1 and T_2, which are in the center and the top of the battery, are higher compared with the thermocouples of T_3 and T_4.

2.3.2. Forced air cooling

The experimental test by forced air cooling is designed to investigate the cooling effect and thermal performance of the heat pipe on the LTO cell. Fig. 6 shows the cell embedded with a flat heat pipe to test the effectiveness of the forced air cooling system. Twelve thermocouples were used to monitor the temperature at different locations of the heat pipe and cell. Fig. 6a shows the schematic front side of the LTO battery cell with the heat pipe and the location of thermocouples. Fig. 6b illustrates the location of thermocouples in the front and backside of the cell that is embedded with a heat pipe. The evaporator section of the heat pipe is connected to the hottest zone of the cell and the condenser section is the rest of the heat pipe which is cooled by forced air cooling with an inlet velocity of 3 m/s. Gap filler with

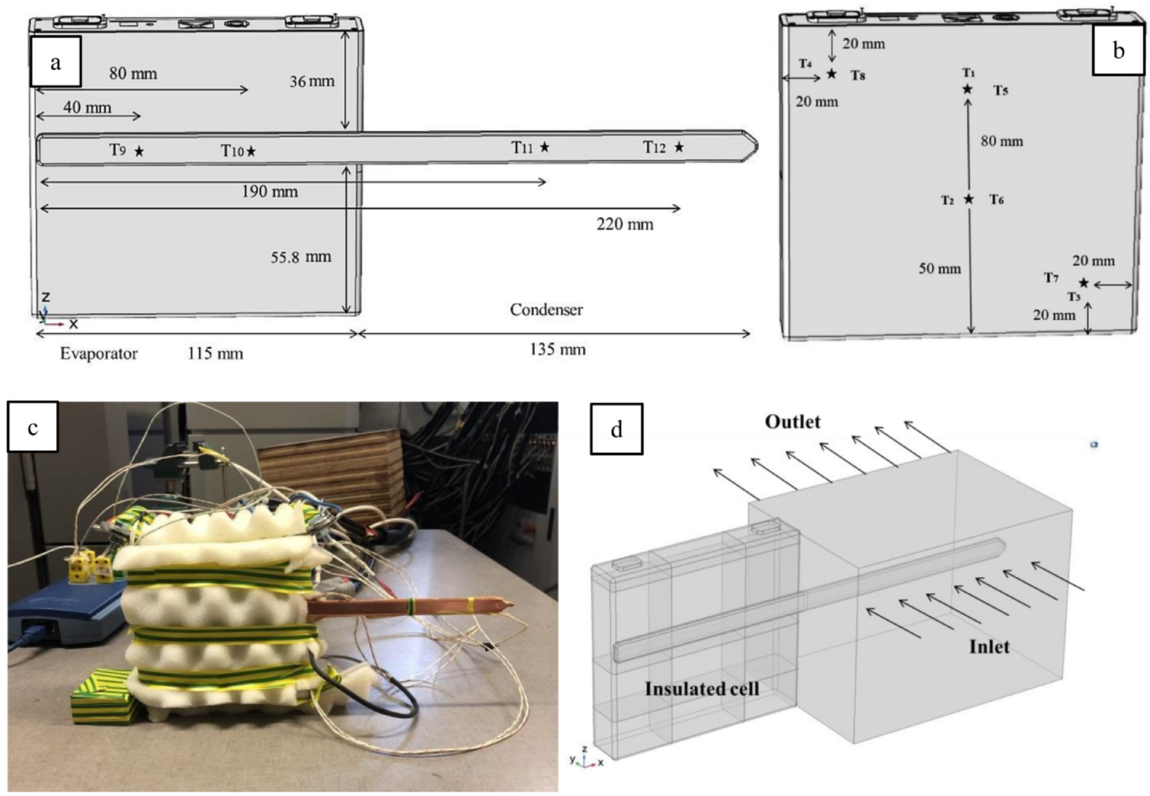

Fig. 6. (a,b) The schematic of battery cell with heat pipe and location of thermocouples of the front (T_1-T_4), backside (T_5-T_8) of the cell and heat pipe (T_9-T_{12}), (c) picture of insulated battery cell with heat pipe and (d) domains and boundary condition of the heat pipe and cell.

thermal conductivity of 3.5 w/m.k is used between the heat pipe and cell to decrease the contact thermal resistance. All surfaces of the cell covered by insulation precisely with the purpose of heat loss reduction. This test aims to find the cooling capacity and consequently the amount of thermal conductivity of the heat pipe using the following equation [59].

$$k_{eff} = \frac{Q_{hp} L_{eff}}{A_h \Delta T} \tag{3}$$

where Q_{hp}, A_h, and ΔT are the heat transferred by the heat pipe, the cross-section area of the heat pipe, and temperature difference of evaporator and condenser of the heat pipe, respectively. It is necessary to mention that four thermocouples were attached on the surface of the heat pipe to have an average temperature for the evaporator and condenser sections. Moreover, the L_{eff} is the effective transport length of the heat pipe that averages as [30]:

$$L_{eff} = \frac{L_e + L_c}{2} + L_a \tag{4}$$

where L_e, L_a and L_c are evaporator, adiabatic and condenser length of the heat pipe, respectively.

The temperature of the insulated cell is measured in 8 points under the 8 C discharging rate. Moreover, the temperature of the insulated cell embedded with a heat pipe is measured while the condenser section of the heat pipe is cooled by a fan with an inlet velocity of 3 m/s.

Fig. 7a shows the temperature difference at the evaporator and condenser of the heat pipe. The average temperature at the evaporator and condenser reached 47.85 °C and 43.49 °C, respectively. Fig. 7b shows the temperature of the front and backside of the insulated cell in the presence of the heat pipe. Explicitly, the average temperature of the front side is lower than the backside due to the effect of the heat pipe. The average temperature of the cell using the heat pipe is 49.39 °C. Fig. 7c also illustrates the temperature of the front and backside of the insulated cell without the heat pipe. It is evident that the average temperature of the cell increased due to the lack of heat pipe. The average temperature of the cell without the heat pipe is 56.91 °C. As the cell is insulated carefully, heat loss is neglected. According to the initial and final temperature of the cell, mass, and the specific heat capacity of the cell, in both tests, the amount of 10.97 W heat was transferred by the heat pipe in the discharging process. As the average of the heat generation by the cell in the 8 C discharging rate is 37.65 W, the amount of 29.1% heat is transferred by a heat pipe. Therefore, based on the parameters and values from Eqs. (2) and (3), the amount of effective thermal conductivity of the heat pipe is calculated as 8212 W/m.K.

3. Simulation

3.1. Battery thermal modeling

The 3D-thermal model has been developed by COMSOL Multiphysics® to reach the thermal behavior of the cell. To define the transient thermal distribution inside the cell, an energy balance equation is used. According to this equation, the amount of thermal energy that is generated by the cell to its surrounding is formulated as follows [60]:

$$mC_p \frac{\partial T}{\partial t} + q_{conv} = k\left[\frac{\partial^2 T}{\partial x^2} + \frac{\partial^2 T}{\partial y^2} + \frac{\partial^2 T}{\partial z^2}\right] + q_g \tag{5}$$

where m, c_p, T, K, and q_g represent the mass, heat capacity, temperature, thermal conductivity, and heat generation, respectively. In the present work, the heat generation of the cell is calculated from the ohmic resistance of the cell and polarization process. Moreover, Eq. (7) uses the tab domain [61].

$$q_g = R_{bt}.\, I^2 + R_1.\, I_1^2 + R_2.\, I_2^2 \tag{6}$$

$$\dot{q} = R_{tab}.\, I^2 \tag{7}$$

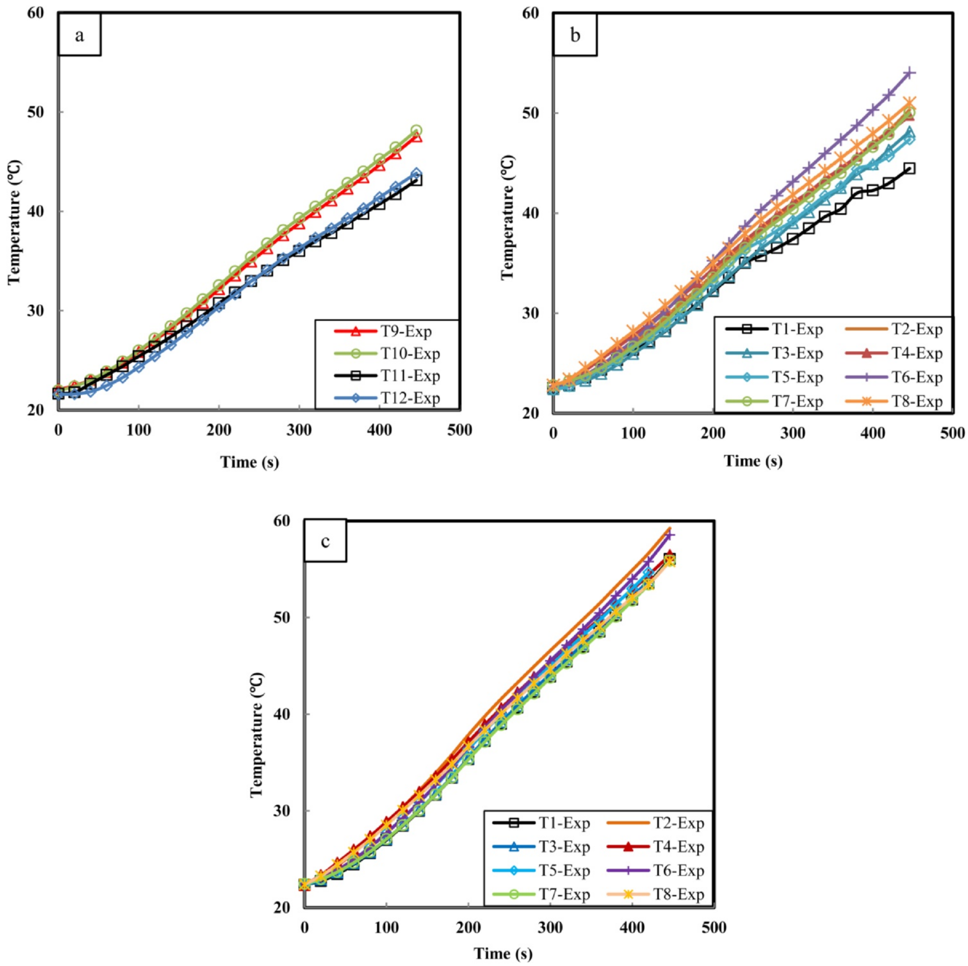

Fig. 7. The temperature of (a) evaporator and condenser of the heat pipe, (b) surface of the insulated cell with heat pipe, and (c) surface of the insulated cell without heat pipe in the 8 C discharging rate.

$$R_{tab} = \rho' \frac{l}{S} \tag{8}$$

wherein, I and R_{bt} represent the current and ohmic resistance of the cell. Besides, for the tab domains R_{tab}, ρ', l, S and are the electrical resistance, resistivity, length, and cross-section of the corresponding tab, respectively. Heat transfer from the cell to the surrounding is also calculated as [62]:

$$q_{conv} = hS(T_{amb} - T) \tag{9}$$

wherein, h and S represent the heat transfer of the coefficient and cross-section area of the cell. Moreover, T and T_{amb} demonstrate the battery and ambient temperature. As it is obvious from Fig. 8 by a thermal camera, there is a non-uniform temperature distribution through the cell domain. Therefore, the localized heat source model has been applied in the cell domain. Thermal infrared (IR) imaging is a useful technique to show, detect average, and measure the temperature of the cell domain especially non-uniform temperature distribution. Based on Fig. 8a, there are two hot zones in the middle of the cell that are specified by red and yellow colors. Therefore, in order to have a precise thermal model, the cell domain is divided into nine domains. The amount of specified heat to each domain is defined based on the average temperature of each zone. The total heat generation in the cell for each zone is formulated as follows:

$$Q_{cell} = Q_1 + Q_2 + \ldots + Q_9 = \alpha Q_{cell} + \beta Q_{cell} + \ldots + \theta Q_{cell} \tag{10}$$

$$\alpha + \beta + \ldots + \theta = 100\% \tag{11}$$

$$Q_1 = \frac{\alpha Q_{cell}}{V_1}, \cdot Q_2 = \frac{\beta Q_{cell}}{V_2}, \ \ldots, \ Q_9 = \frac{\theta Q_{cell}}{V_9} \tag{12}$$

where the α, V_1, β, V_2, …, θ, V_9 are the percentage of total heat generation and volume of each zone respectively. Fig. 8b shows the simulation of the cell utilizing the nine localized heat sources and their percentages. Moreover, Fig. 8c illustrates the simulation of the insulated cell with a heat pipe in forced air cooling.

3.2. Validation of the thermal model for natural and forced-air cooling in cell level

The transient simulation was performed using the measured transient wall temperature of the heat pipe along the evaporator and condenser section and cell surface. In order to do the validation and show the accuracy of the numerical method, the temperature of thermocouples of T_2 and T_4 for natural air cooling (Fig. 9a,b), T_1 and T_6 for forced air cooling (Fig. 9e), and T_9-T_{12} for the flat heat pipe (Fig. 9b,c) during discharging mode are compared with the simulation results. The average relative errors for T_2, T_4, T_1, and T_6 are 1.2%, 4.4%, 3.2%, and 1% respectively within an acceptable error range [63]. Moreover, the average errors for thermocouples of T_9 to T_{12} are 2.6%, 4.2%, 1%, and 1% respectively. The locations of thermocouples on the cell and heat pipe are shown in Figs. 6 and 4 respectively. As can be seen in Fig. 9, there is an acceptable agreement by the comparison of simulation and experimental data during the discharge process. Such a good agreement proves the accuracy of the numerical simulations and lays the basis for the following prediction of the thermal behavior of the cells and heat

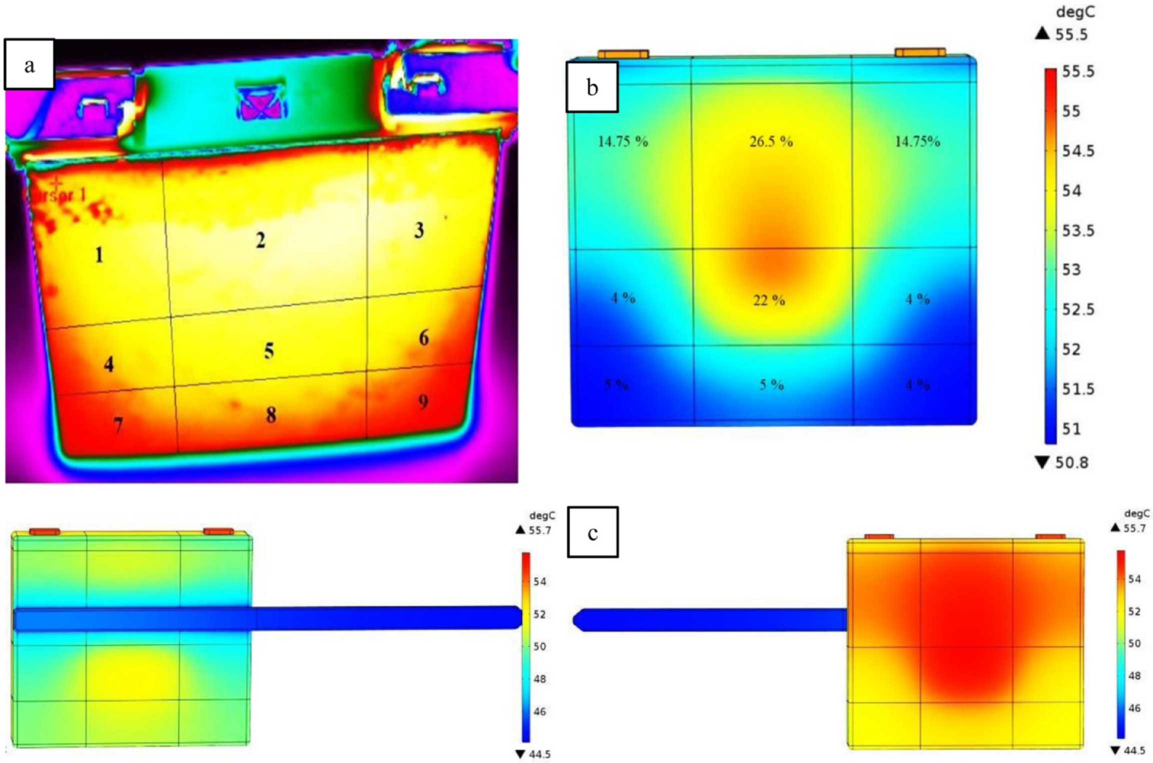

Fig. 8. The picture of (a) the thermal camera with the classified nine zones in natural air cooling, (b) the simulation of the cell, and (c) the front and back-side of the insulated cell with the heat pipe in 8 C discharging rate.

pipes in the actual module. In this model, the heat pipe is replaced by a solid region, and the effective thermal conductivity of components is used in the simulation [28,40,59,64].

3.3. Conceptual design of LCHP

After single-cell analysis, we developed the concept for cooling at the module level. The LTO module is comprised of 15 cells with 345 kWh capacity, further specifications are summarized in Table 4.

Explicitly choosing a suitable cooling system for the module is a big challenge. The air cooling system is considered the most common cooling system by designers and manufacturers for thermal management of Li-ion batteries due to its simplicity. Nevertheless, air cooling is not an appropriate solution for stressful and abuse conditions [65,66], particularly during high rates of charging/discharging due to the low specific heat capacity of air. Therefore, in the current study, the module is equipped with liquid cooling and LCHP. LCHP is a combination of the liquid cooling system and the heat pipe. Generally, the liquid cooling system is the most appropriate, favorable, and applied cooling system with compact design and superior cooling performance in cooling applications. Moreover, the heat pipe, as a superconductor has been used widely for battery TMS. Therefore, a combination of them in LCHP presents an ideal and efficient cooling system for high current applications. The experimental tests to find the thermal performance of the heat pipe was done and shown in Fig. 6.

3.3.1. Geometry model of the module equipped with LCHP

At this stage, the magnitude of temperature rise in the actual battery module is solved numerically to calculate the transient temperature rise of cells. Fig. 10 shows the LCHP for an LTO prismatic battery module. In this design, the module sandwiched by cooling plates whiles the heat pipes connected to the cells and welded to the cooling plates. It is important to note that for every cell only a flat heat pipe is used. Consistent with Fig. 8, the heat pipes are placed in the most effective position (hottest zone) to maximize the performance of the cooling system. The cooling system is designed for the thermal management of the battery module during the 8 C discharging rate. Every cooling plate has three direct inlets of water with an inlet velocity of 1 m/s which is connected to the heat pipes. During the charging/discharging, the heat generated within the cells is conducted to the cooling plates. Moreover, some parts of heat generation through evaporator sections of the heat pipes are transferred to condenser sections (plates) and from there to the circulating coolant.

3.3.2. Governing equations

The numerical heat transfer analysis using COMSOL Multiphysics of the proposed system requires a mathematical model to explain the physics of the problem. Below are the governing equations, including continuity, momentum, and energy required for the analysis:

$$\frac{\partial u_i}{\partial x_i} = 0 \tag{13}$$

$$\rho\left(\frac{\partial u_i}{\partial t} + u_j\frac{\partial u_i}{\partial x_j}\right) = -\frac{\partial p}{\partial x_i} + \mu\frac{\partial^2 u_i}{\partial {x_j}^2} + \rho \tag{14}$$

$$\rho C_p\left(\frac{\partial T}{\partial t} + u_j\frac{\partial T}{\partial x_j}\right) = \lambda\frac{\partial^2 T}{\partial {x_j}^2} + \dot{q} \tag{15}$$

In Eq. (16) the latter part of the equation $\dot{q}$ denotes the volumetric heat generation rate in battery cells which is calculated as follow: [67]

$$\dot{q} = \frac{R_{bt}.\ I^2}{\mathrm{v}} \tag{16}$$

Where,

U = fluid velocity
ρ = density of fluid
p = pressure
μ = fluid viscosity

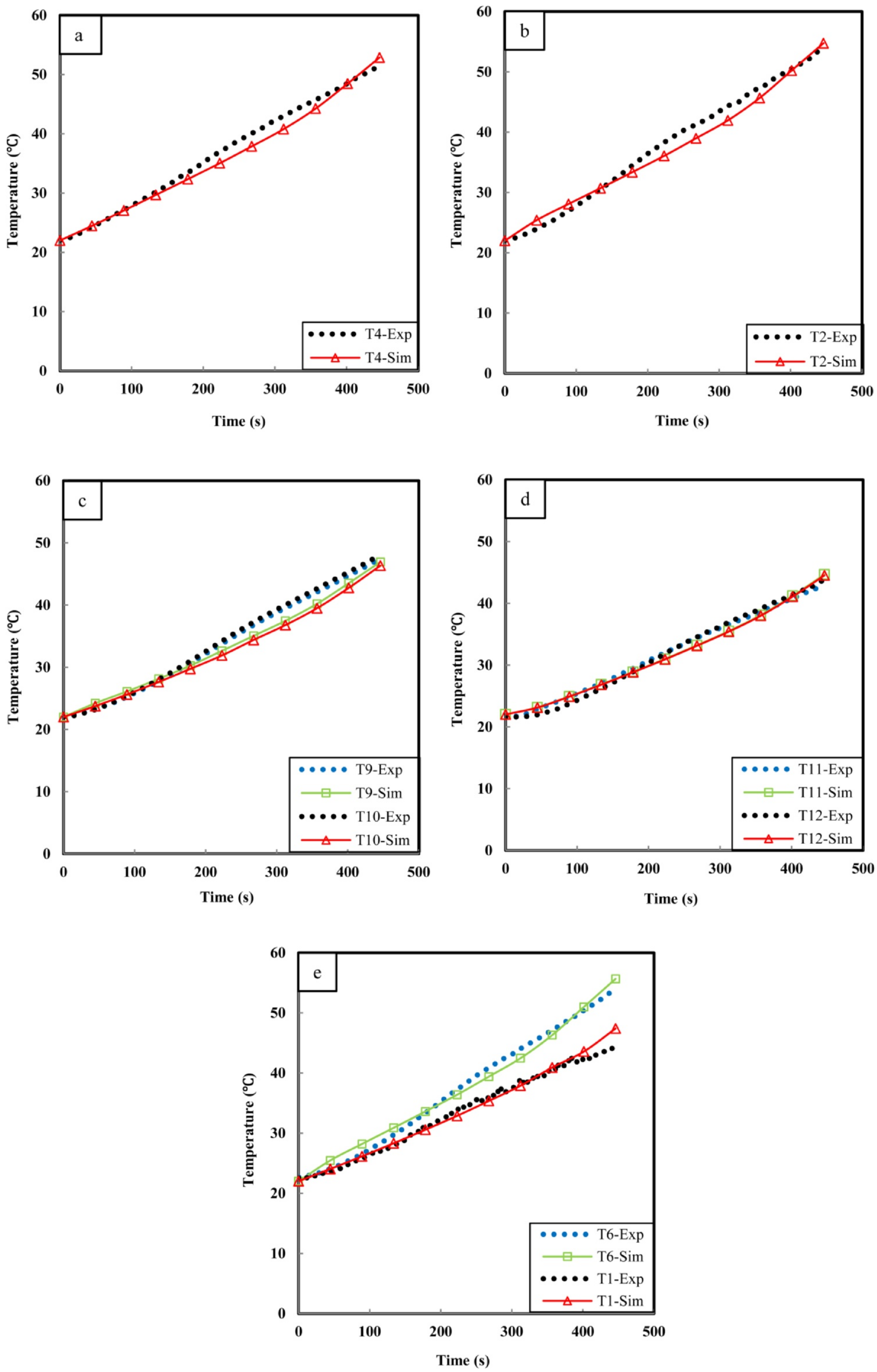

Fig. 9. Thermal model validation of (a) natural air cooling for T_4 and (b) T_2, (c,d) forced air cooling for evaporator and condenser of the heat pipe, and (e) surface of the insulated cell equipped with heat pipe in the 8 C discharging rate (Sim: Simulation).

g_i = the considered body force (in natural air cooling)
C_p = specific heat capacity
λ = heat generation
R_{bt} = total internal resistance of the cell
I = electrical current
v = volume of the battery cells

3.3.3. Boundary condition, meshing, and grid independence analysis for LCHP

The boundary conditions for the governing equations are related to the operation of the LCHP. In practice, the heat pipe is attached to the heat source to receive some part of the heat and reject it by fluid flow through the cooling plates. In this study, for the proposed system, the initial temperature of the battery, the cooling plate, and the coolant are set to 22 °C. Besides, coolant inlet velocity and temperature are

Table 4
The specifications of the LTO module.

Parameter	Value
Number of cells in series	15
Nominal voltage of the module (V)	34.5
Weight (kg)	8.25
Volume (L)	3.9
Stored energy in the module (kWh)	345

turbulent, and uniform, in which the inlet velocity of the coolant is set to 1 m/s, and the outlet is assumed as the ambient pressure. The turbulence model selected is the low Re k-ε because of high accuracy for heat transfer [68]. The governing equation is based on the following k and ε equations [69],

$$\rho\frac{Dk}{Dt} = \frac{\partial}{\partial x_i}\left[\left(\mu + \frac{\mu_t}{\partial_k}\right)\frac{dk}{dx_i}\right] + G_k - \rho\varepsilon - \mathrm{D} \tag{17}$$

$$\rho\frac{D\varepsilon}{Dt} = \frac{\partial}{\partial x_i}\left[\left(\mu + \frac{\mu_t}{\partial_\varepsilon}\right)\frac{d\varepsilon}{dx_i}\right] + \frac{c_{\varepsilon1}\, f_1\, G_k\, \varepsilon}{k} - \frac{c_{\varepsilon2}\, f_1\, \varepsilon^2}{k} \tag{18}$$

Where,

$$G_k{\cdot}={\cdot}\mu_t S^2{\cdot}={\cdot}0.5\mu_t\left(\frac{\partial u_i}{\partial x_j} + \frac{\partial u_j}{\partial x_i}\right)^2 \text{and} \mu_t{\cdot}={\cdot}C_\mu\, \rho\, f_\mu \frac{\mathrm{k}^2}{\varepsilon} \tag{19}$$

In the current simulation, the thermal radiation transfer was assumed to be negligible and was not taken into account. Besides, due to the different geometrical scales in the current model, the simulation process is very time-consuming. Therefore, the grid independency test was done to refine the grid size while the results are not changed by further refinement of the mesh. Fig. 11 shows the maximum temperature of the module to estimate the independence of the grid number. In this case, when the grid number varies from 975,136 to 1,218,808, the result differs only 0.1 °C. Therefore because of computational time-saving, the grid number of 975,136 is chosen for the module simulation.

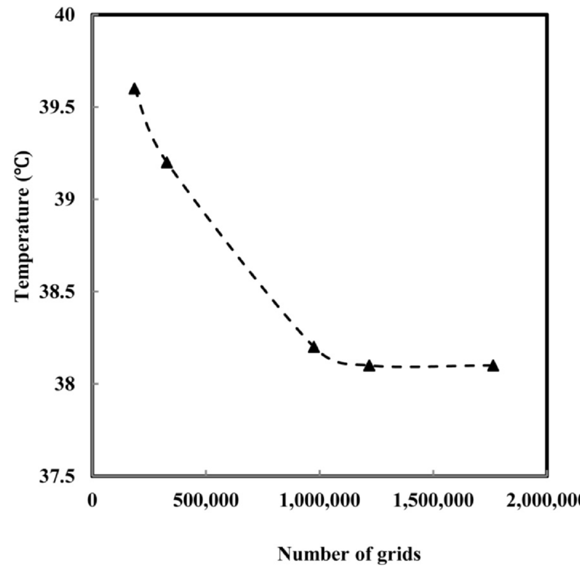

Fig. 11. Grid number independency test.

3.3.4. Validation of the liquid cooling system in the cell level

After cell level study in natural and forced air cooling, to predict the performance of the liquid cooling system in the module level, we have built a model of the module in COMSOL Multiphysics. In order to validate the accuracy of the liquid cooling numerical results, the experimental [70] maximum cell temperature distribution under 5 C discharging rate is compared with the simulation results. As can be seen in Fig. 12 there is an acceptable trend agreement between the

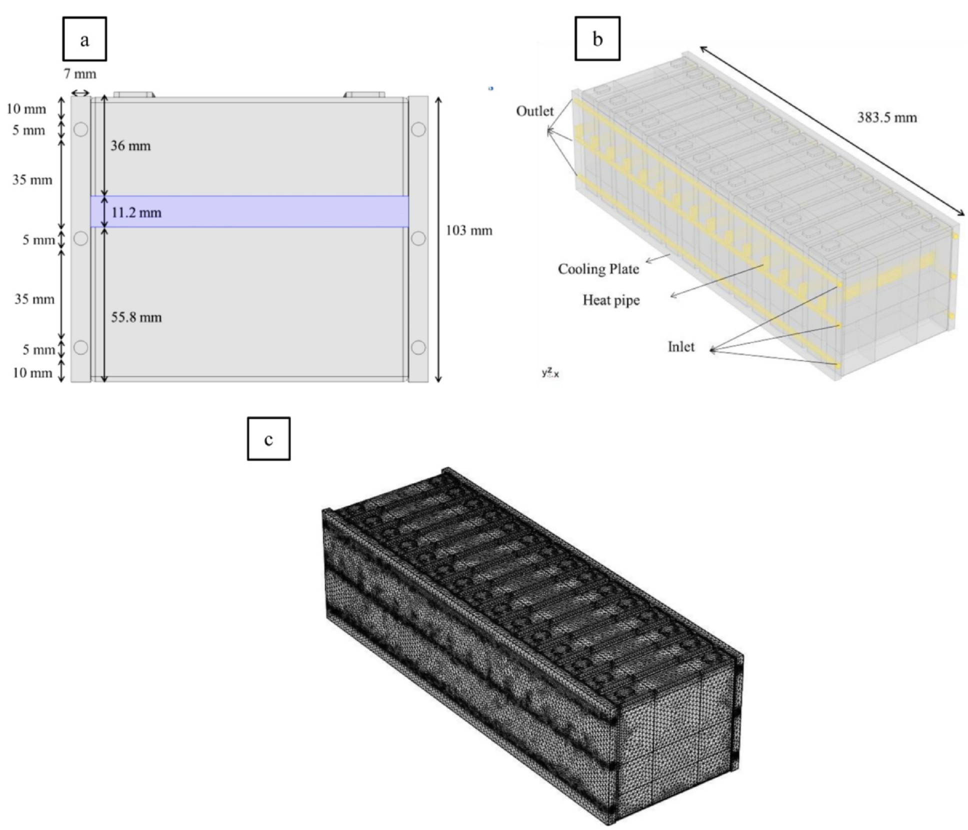

Fig. 10. (a,b) Schematic and dimension of the cooling plates and heat pipes for the battery module, and (c) mesh distribution in the battery module.

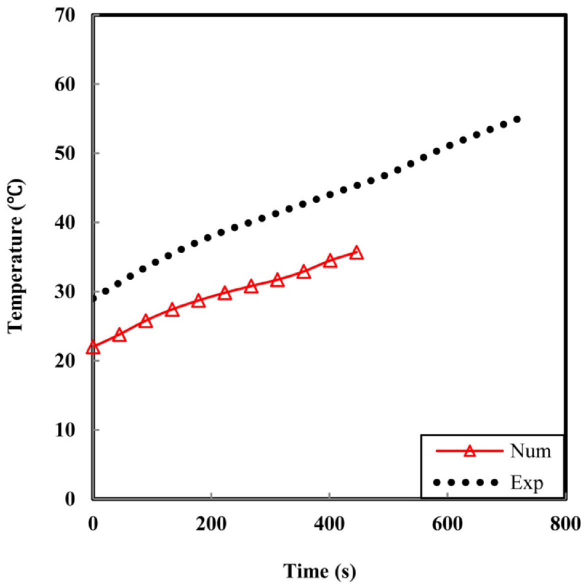

Fig. 12. Thermal model validation of a liquid cooling system with experimental results.

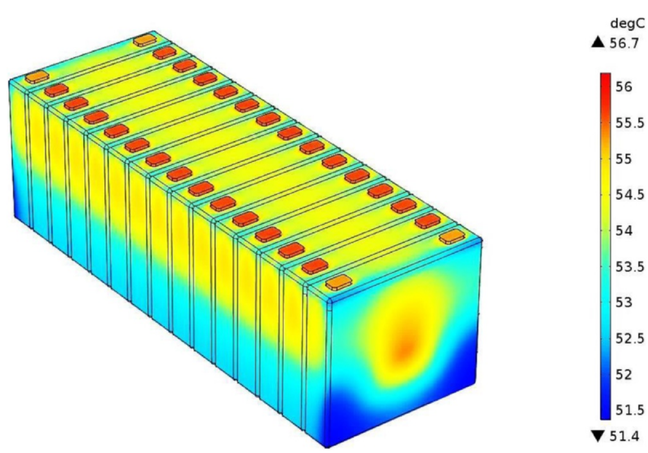

Fig. 13. Temperature contour of the module in natural air cooling.

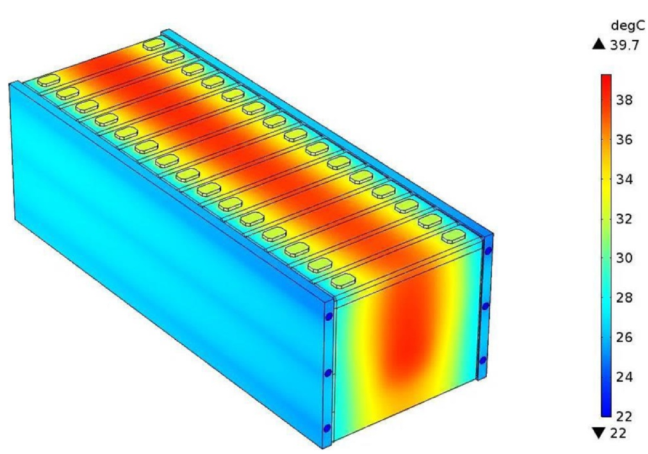

Fig. 14. Temperature contour of the module in liquid side cooling.

experimental data and simulation results. It is necessary to mention that the difference in temperature and time is due to the different initial temperatures and rate of discharge. The validation is done at the cell level, which can be extended to the module as the cell, cooling system and boundary conditions are the same.

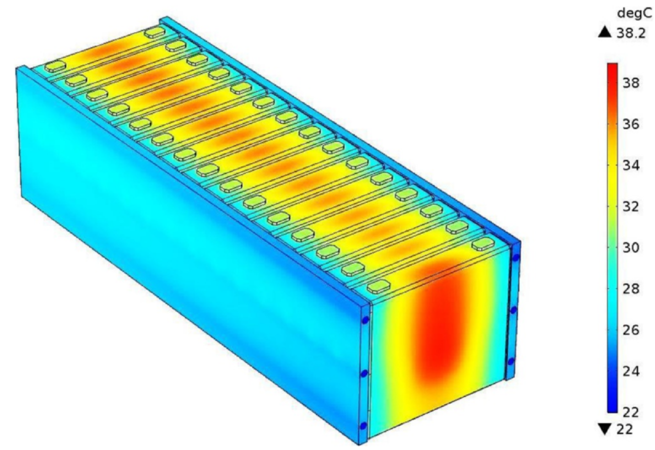

Fig. 15. Temperature contour of the module in liquid side cooling and heat pipe.

3.3.5. Simulation results and discussion

To estimate the amount of temperature rise in the actual battery pack, a 3D thermal model of a module comprising of 15 cells was developed and solved numerically by COMSOL to predict the transient temperature rise of cells. For the purpose of comparison, the maximum temperature of the module in the same initial condition for natural and forced air cooling has been considered. In this section, the thermal behavior of the module is subjected to the four cooling strategies and boundary conditions in the 8 C discharging rate. The strategies comprise as follows:

Study the temperature of the module in natural air cooling at an initial temperature of 22 °C.

The first phase to study the thermal performance of the module is the consideration of natural air cooling. In this passive method, the module is cooled without consuming any external energy. As indicated in Fig. 13 for natural air cooling the produced heat from the module increases the temperature to 56.7 °C at the end of the discharging rate period. Moreover, the heat is more concentrated in the middle and tabs of the module. Therefore, due to the excessive heat generation by the module, it needs a cooling system.

Study the temperature of the module in sandwich side liquid cooling at an initial temperature of 22 °C and inlet velocity of 1 m/s.

According to the physical properties of the LTO prismatic cell, sandwich side liquid cooling is a suitable cooling method. As it is clear from Fig. 14, the maximum temperature of the module decreased tremendously compare with the natural air cooling and reached 39.7 °C. Moreover, the temperature of the tabs controlled and reached almost 33 °C. The hottest area migrated and separated from the center to the top of the cell by the effect of cooling plates. The cooling system affords the safe operation range of Li-ion batteries (25–40 °C) [11] however, the maximum temperature and uniformity can be improved.

Study the temperature of the module in LCHP at an initial temperature of 22 °C and inlet velocity of 1m/s.

As revealed in Fig. 14, when a module is subjected to cooling on both sides by cooling plates, the maximum temperature of the module is controlled in a safe range at the end of the discharging process. This shows that the current cooling plates meet the requirements of the module thermal management. Nevertheless, in order to increase the temperature uniformity and further performance improvement of the current cooling plates, a number of heat pipes are employed. As can be seen in Fig. 15 the maximum temperature of the module decrease 1.5 °C and reached 38.2 °C. Moreover, temperature uniformity has been improved relatively.

Study the temperature of the module in LCHP at an initial temperature of

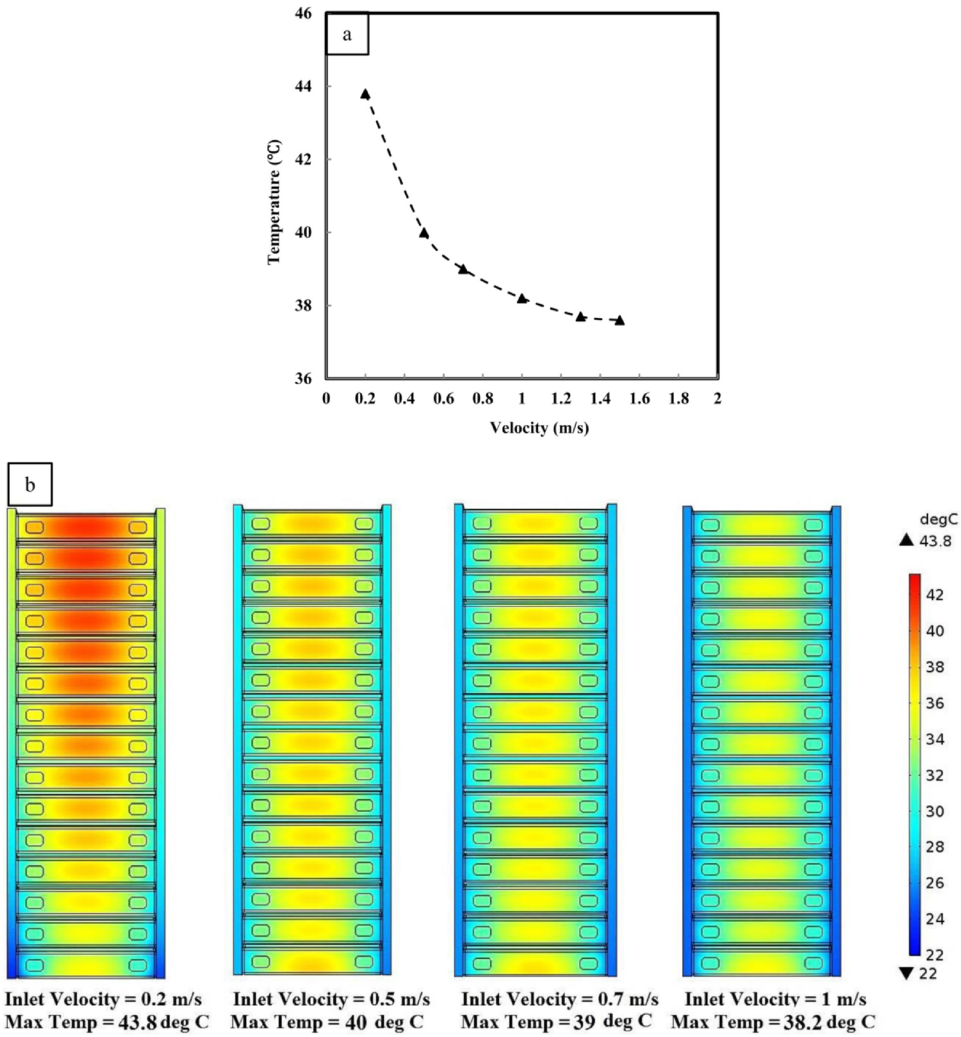

Fig. 16. Temperature graph and contours of the module with different inlet velocities (a) from 0.2–1.5 m/s and (b) from 0.2–1 m/s.

22 °C and different inlet velocity.

Fig. 16a shows a study on varying the coolant velocity, from the maximum temperatures of the module. As it is obvious, the coolant velocity has a direct influence on the temperature behavior of the module. The temperature varying from 43.8 °C to 37.6 °C by different velocity from 0.2 m/s to 1.5 m/s respectively. Explicitly by the velocity of 1 m/s the temperature reached 38.2 °C that is in a safe range [11] for balance between performance and life of Li-ion battery. Therefore, higher velocities are a more cost-effective velocity for the present design.

Additionally, Fig. 16b illustrates the further study on temperature contours of the module in the XY plane with the inlet velocities of 0.2 m/s to 1 m/s at the end of the discharging process. For the velocity of 0.2 m/s, the temperature is non-uniform and increased from the inlet to the outlet of liquid cooling plates. For the velocity of 0.5–1 m/s the maximum temperature decreased and temperature uniformity increased for the hole of the module. In fact, the temperature sharply reduces and reaches a reasonably steady state after the velocity of the 0.5 m/s.

4. Summary and outlook

4.1. Conclusion

The efforts of this study were undertaken to consider the cooling effect of the heat pipe on the LTO prismatic cell/module in high current discharging. In order to achieve this aim, several studies were performed on different boundary conditions and design as follows:

- The temperature of the cell in natural air cooling for the initial temperatures of 22 °C in the 8 C discharging rate is considered.
- The thermal distribution inside the cell is monitored using the thermal camera. Through thermal analysis, only one heat pipe is placed in the most effective position for maximizing the performance of the cooling system and decreases the weight and volume of the cooling system.
- The cooling effect of the flat heat pipe is evaluated experimentally with LTO prismatic cell in the 8C discharging rate. It was found that the single heat pipe provided up to 29.1% of the required cooling load. Also, the thermal conductivity of the heat pipe is calculated.
- The numerical results are validated with the experimental results. In order to have a precise thermal model, using the COMSOL Multiphysics® the cell domain is divided into nine heat source domains.
- For optimization, a module consisting of 15 cells equipped with liquid cooling and LCHP is simulated. It was found that the liquid cooling system and LCHP compared with natural air cooling reduced the maximum module temperature by 29.9% and 32.6%, respectively.

4.2. Future work

The temperature gradient influences the performance of the heat pipe cooling. The cooling system can maintain the cell/module at an acceptable temperature; however, the different gradient may affect the cooling performance of the TMS. Under real operating conditions, it is not expected for the cooling system to run continuously at such a steep gradient. Therefore, this limitation does not compromise the suitability of this cooling system as a battery thermal management solution. The only point that needs to be further discussed is the consideration of such a condition on the temperature uniformity of the module.

Declaration of Competing Interest

The authors declare that they have no known competing financial interests or personal relationships that could have appeared to influence the work reported in this paper.

Acknowledgment

'This paper was developed under the framework of the SELFIE project. This project has received funding from the European Union's Horizon 2020 research and innovation program under Grant Agreement Nr. 824290.' Further, the authors acknowledge 'Flanders Make' for the support to MOBI research group.

References

[1] M. Lu, X. Zhang, J. Ji, X. Xu, Y. Zhang, Research progress on power battery cooling technology for electric vehicles, J. Energy Storage 27 (2020) 101155, , https://doi.org/10.1016/J.EST.2019.101155.
[2] L.H. Saw, H.M. Poon, H.S. Thiam, Z. Cai, W.T. Chong, N.A. Pambudi, Y.J. King, Novel thermal management system using mist cooling for lithium-ion battery packs, Appl. Energy 223 (2018) 146–158, https://doi.org/10.1016/J.APENERGY.2018.04.042.
[3] X. Xu, W. Li, B. Xu, J. Qin, Numerical study on a water cooling system for prismatic $LiFePO_4$ batteries at abused operating conditions, Appl. Energy 250 (2019) 404–412, https://doi.org/10.1016/J.APENERGY.2019.04.180.
[4] S.H. Hong, D.S. Jang, S. Park, S. Yun, Y. Kim, Thermal performance of direct two-phase refrigerant cooling for lithium-ion batteries in electric vehicles, Appl. Therm. Eng. 173 (2020) 115213, , https://doi.org/10.1016/J.APPLTHERMALENG.2020.115213.
[5] Y. Ye, Y. Shi, A.A.O. Tay, Electro-thermal cycle life model for lithium iron phosphate battery, J. Power Sources 217 (2012) 509–518, https://doi.org/10.1016/J.JPOWSOUR.2012.06.055.
[6] S. Zhang, R. Zhao, J. Liu, J. Gu, Investigation on a hydrogel based passive thermal management system for lithium ion batteries, Energy 68 (2014) 854–861, https://doi.org/10.1016/J.ENERGY.2014.03.012.
[7] Y. Ye, Y. Shi, A.A.O. Tay, Electro-thermal cycle life model for lithium iron phosphate battery, J. Power Sources 217 (2012) 509–518, https://doi.org/10.1016/J.JPOWSOUR.2012.06.055.
[8] Q. Wang, B. Jiang, B. Li, Y. Yan, A critical review of thermal management models and solutions of lithium-ion batteries for the development of pure electric vehicles, Renew. Sustain. Energy Rev. 64 (2016) 106–128, https://doi.org/10.1016/J.RSER.2016.05.033.
[9] Q. Wang, P. Ping, X. Zhao, G. Chu, J. Sun, C. Chen, Thermal runaway caused fire and explosion of lithium ion battery, J. Power Sources 208 (2012) 210–224, https://doi.org/10.1016/J.JPOWSOUR.2012.02.038.
[10] L.H. Saw, Y. Ye, M.C. Yew, W.T. Chong, M.K. Yew, T.C. Ng, Computational fluid dynamics simulation on open cell aluminium foams for Li-ion battery cooling system, Appl. Energy 204 (2017) 1489–1499, https://doi.org/10.1016/J.APENERGY.2017.04.022.
[11] T.M. Bandhauer, S. Garimella, T.F. Fuller, A critical review of thermal issues in lithium-ion batteries, J. Electrochem. Soc. (2011) 158, https://doi.org/10.1149/1.3515880.
[12] L.H. Saw, Y. Ye, A.A.O. Tay, W.T. Chong, S.H. Kuan, M.C. Yew, Computational fluid dynamic and thermal analysis of lithium-ion battery pack with air cooling, Appl. Energy 177 (2016) 783–792, https://doi.org/10.1016/j.apenergy.2016.05.122.
[13] A.A. Pesaran, Battery thermal models for hybrid vehicle simulations, J. Power Sources 110 (2002) 377–382, https://doi.org/10.1016/S0378-7753(02)00200-8.
[14] D. Karimi, H. Behi, J. Jaguemont, M. El Baghdadi, J. Van Mierlo, O. Hegazy, Thermal concept design of mosfet power modules in inverter subsystems for electric vehicles, (2019).
[15] H. Behi, M. Ghanbarpour, M. Behi, Investigation of PCM-assisted heat pipe for electronic cooling, Appl. Therm. Eng. 127 (2017) 1132–1142, https://doi.org/10.1016/j.applthermaleng.2017.08.109.
[16] M. Behi, S.A. Mirmohammadi, M. Ghanbarpour, H. Behi, B. Palm, Evaluation of a novel solar driven sorption cooling/heating system integrated with PCM storage compartment, Energy 164 (2018) 449–464, https://doi.org/10.1016/J.ENERGY.2018.08.166.
[17] M. Behi, M. Shakorian-poor, S.A. Mirmohammadi, H. Behi, J.I. Rubio, N. Nikkam, M. Farzaneh-Gord, Y. Gan, M. Behnia, Experimental and numerical investigation on hydrothermal performance of nanofluids in micro-tubes, Energy 193 (2020) 116658, , https://doi.org/10.1016/J.ENERGY.2019.116658.
[18] H. Park, A design of air flow configuration for cooling lithium ion battery in hybrid electric vehicles, J. Power Sources 239 (2013) 30–36, https://doi.org/10.1016/J.JPOWSOUR.2013.03.102.
[19] R. Liu, J. Chen, J. Xun, K. Jiao, Q. Du, Numerical investigation of thermal behaviors in lithium-ion battery stack discharge, Appl. Energy 132 (2014) 288–297, https://doi.org/10.1016/J.APENERGY.2014.07.024.
[20] J. Xun, R. Liu, K. Jiao, Numerical and analytical modeling of lithium ion battery thermal behaviors with different cooling designs, J. Power Sources 233 (2013) 47–61, https://doi.org/10.1016/J.JPOWSOUR.2013.01.095.
[21] Y. Lai, W. Wu, K. Chen, S. Wang, C. Xin, A compact and lightweight liquid-cooled thermal management solution for cylindrical lithium-ion power battery pack, Int. J. Heat Mass Transf. 144 (2019) 118581, , https://doi.org/10.1016/J.IJHEATMASSTRANSFER.2019.118581.
[22] H. Zhou, F. Zhou, Q. Zhang, Q. Wang, Z. Song, Thermal management of cylindrical lithium-ion battery based on a liquid cooling method with half-helical duct, Appl. Therm. Eng. 162 (2019) 114257, , https://doi.org/10.1016/J.APPLTHERMALENG.2019.114257.
[23] Z. Sun, R. Fan, F. Yan, T. Zhou, N. Zheng, Thermal management of the lithium-ion battery by the composite PCM-Fin structures, Int. J. Heat Mass Transf. 145 (2019) 118739, , https://doi.org/10.1016/J.IJHEATMASSTRANSFER.2019.118739.
[24] Y. Ye, L.H. Saw, Y. Shi, A.A.O. Tay, Numerical analyses on optimizing a heat pipe thermal management system for lithium-ion batteries during fast charging, Appl. Therm. Eng. 86 (2015) 281–291, https://doi.org/10.1016/J.APPLTHERMALENG.2015.04.066.
[25] D. Dan, C. Yao, Y. Zhang, H. Zhang, Z. Zeng, X. Xu, Dynamic thermal behavior of micro heat pipe array-air cooling battery thermal management system based on thermal network model, Appl. Therm. Eng. 162 (2019) 114183, , https://doi.org/10.1016/J.APPLTHERMALENG.2019.114183.
[26] Z. Rao, Y. Huo, X. Liu, Experimental study of an OHP-cooled thermal management system for electric vehicle power battery, Exp. Therm. Fluid Sci. 57 (2014) 20–26, https://doi.org/10.1016/J.EXPTHERMFLUSCI.2014.03.017.
[27] B. Coleman, J. Ostanek, J. Heinzel, Reducing cell-to-cell spacing for large-format lithium ion battery modules with aluminum or PCM heat sinks under failure conditions, Appl. Energy 180 (2016) 14–26, https://doi.org/10.1016/J.APENERGY.2016.07.094.
[28] H. Behi, Experimental and numerical study on heat pipe assisted PCM storage system, (2015).
[29] L.L. VasilievMicro and miniature heat pipes–Electronic component coolers, Appl. Therm. Eng 28 (4) (2008) 266–273, https://doi.org/10.1016/J.APPLTHERMALENG.2006.02.023.
[30] M. Ghanbarpour, Investigation of thermal performance of cylindrical heat pipes operated with nanofluids, 2017.
[31] A.R.M. Siddique, S. Mahmud, B. Van Heyst, A comprehensive review on a passive (phase change materials) and an active (thermoelectric cooler) battery thermal management system and their limitations, J. Power Sources 401 (2018) 224–237, https://doi.org/10.1016/J.JPOWSOUR.2018.08.094.
[32] L. Feng, S. Zhou, Y. Li, Y. Wang, Q. Zhao, C. Luo, G. Wang, K. Yan, Experimental investigation of thermal and strain management for lithium-ion battery pack in heat pipe cooling, J. Energy Storage 16 (2018) 84–92, https://doi.org/10.1016/j.est.2018.01.001.
[33] Q. Wang, B. Jiang, Q.F. Xue, H.L. Sun, B. Li, H.M. Zou, Y.Y. Yan, Experimental investigation on EV battery cooling and heating by heat pipes, Appl. Therm. Eng. 88 (2015) 54–60, https://doi.org/10.1016/J.APPLTHERMALENG.2014.09.083.
[34] H. Fathabadi, High thermal performance lithium-ion battery pack including hybrid active–passive thermal management system for using in hybrid/electric vehicles, Energy 70 (2014) 529–538, https://doi.org/10.1016/J.ENERGY.2014.04.046.
[35] H. Liu, Z. Wei, W. He, J. Zhao, Thermal issues about Li-ion batteries and recent progress in battery thermal management systems: a review, Energy Convers. Manag. 150 (2017) 304–330, https://doi.org/10.1016/J.ENCONMAN.2017.08.016.
[36] W. Wu, X. Yang, G. Zhang, K. Chen, S. Wang, Experimental investigation on the thermal performance of heat pipe-assisted phase change material based battery thermal management system, Energy Convers. Manag. 138 (2017) 486–492, https://doi.org/10.1016/J.ENCONMAN.2017.02.022.
[37] D. Karimi, H. Behi, J. Jaguemont, M.A. Sokkeh, T. Kalogiannis, M.S. Hosen, M. Berecibar, J. Van Mierlo, Thermal performance enhancement of phase change material using aluminum-mesh grid foil for lithium-capacitor modules, J. Energy Storage 30 (2020) 101508, , https://doi.org/10.1016/j.est.2020.101508.
[38] A. Faghri, Heat Pipe Science and Technology, Taylor & Francis, 1995.
[39] D. Dan, C. Yao, Y. Zhang, H. Zhang, Z. Zeng, X. Xu, Dynamic thermal behavior of micro heat pipe array-air cooling battery thermal management system based on thermal network model, Appl. Therm. Eng. 162 (2019) 114183, , https://doi.org/10.1016/J.APPLTHERMALENG.2019.114183.
[40] H. Behi, D. Karimi, M. Behi, M. Ghanbarpour, J. Jaguemont, M. Akbarzadeh Sokkeh, F. Heidari Gandoman, M. Berecibar, J. Van Mierlo, A new concept of thermal management system in Li-ion battery using air cooling and heat pipe for electric vehicles, Appl. Therm. Eng. (2020) 115280, , https://doi.org/10.1016/J.APPLTHERMALENG.2020.115280.
[41] Z. Rao, S. Wang, M. Wu, Z. Lin, F. Li, Experimental investigation on thermal

management of electric vehicle battery with heat pipe, Energy Convers. Manag. 65 (2013) 92–97, https://doi.org/10.1016/J.ENCONMAN.2012.08.014.
[42] L. Feng, S. Zhou, Y. Li, Y. Wang, Q. Zhao, C. Luo, G. Wang, K. Yan, Experimental investigation of thermal and strain management for lithium-ion battery pack in heat pipe cooling, J. Energy Storage 16 (2018) 84–92, https://doi.org/10.1016/J.EST.2018.01.001.
[43] C. Botsford, O. Ev, Fast Charging vs . Slow Charging : Pros and cons for the New Age of Electric Vehicles 20 Years of EV History 1989 to 2009, (2009) 1–9.
[44] Y. Ye, Y. Shi, L.H. Saw, A.A.O. Tay, Performance assessment and optimization of a heat pipe thermal management system for fast charging lithium ion battery packs, Int. J. Heat Mass Transf. 92 (2016) 893–903, https://doi.org/10.1016/J.IJHEATMASSTRANSFER.2015.09.052.
[45] Y. Ye, L.H. Saw, Y. Shi, A.A.O. Tay, Numerical analyses on optimizing a heat pipe thermal management system for lithium-ion batteries during fast charging, Appl. Therm. Eng. 86 (2015) 281–291, https://doi.org/10.1016/J.APPLTHERMALENG.2015.04.066.
[46] D. Dan, C. Yao, Y. Zhang, H. Zhang, Z. Zeng, X. Xu, Dynamic thermal behavior of micro heat pipe array-air cooling battery thermal management system based on thermal network model, Appl. Therm. Eng. 162 (2019) 114183, , https://doi.org/10.1016/J.APPLTHERMALENG.2019.114183.
[47] J. Liang, Y. Gan, Y. Li, M. Tan, J. Wang, Thermal and electrochemical performance of a serially connected battery module using a heat pipe-based thermal management system under different coolant temperatures, Energy (2019), https://doi.org/10.1016/j.energy.2019.116233.
[48] A. Wei, J. Qu, H. Qiu, C. Wang, G. Cao, Heat transfer characteristics of plug-in oscillating heat pipe with binary-fluid mixtures for electric vehicle battery thermal management, Int. J. Heat Mass Transf. 135 (2019) 746–760, https://doi.org/10.1016/j.ijheatmasstransfer.2019.02.021.
[49] S. Goutam, J.M. Timmermans, N. Omar, P.Van den Bossche, J. Van Mierlo, Comparative study of surface temperature behavior of commercial li-ion pouch cells of different chemistries and capacities by infrared thermography, Energies 8 (2015) 8175–8192, https://doi.org/10.3390/en8088175.
[50] K.H. Do, S.J. Kim, S.V. Garimella, A mathematical model for analyzing the thermal characteristics of a flat micro heat pipe with a grooved wick, Int. J. Heat Mass Transf. 51 (2008) 4637–4650, https://doi.org/10.1016/J.IJHEATMASSTRANSFER.2008.02.039.
[51] S.J. Kim, J. Ki Seo, K. Hyung Do, Analytical and experimental investigation on the operational characteristics and the thermal optimization of a miniature heat pipe with a grooved wick structure, Int. J. Heat Mass Transf. 46 (2003) 2051–2063, https://doi.org/10.1016/S0017-9310(02)00504-5.
[52] M. Ghanbarpour, N. Nikkam, R. Khodabandeh, M.S. Toprak, Improvement of heat transfer characteristics of cylindrical heat pipe by using SiC nanofluids, Appl. Therm. Eng. 90 (2015) 127–135, https://doi.org/10.1016/J.APPLTHERMALENG.2015.07.004.
[53] Ronald Stordahl, Digi-Key Electronics Company, (n.d.). https://www.digikey.be/products/en/fans-thermal-management/thermal-heat-pipes-vapor-chambers/977?k=heatpipe.
[54] K.-T. Lin, S.-C. Wong, Performance degradation of flattened heat pipes, Appl. Therm. Eng. 50 (2013) 46–54, https://doi.org/10.1016/J.APPLTHERMALENG.2012.06.001.
[55] C.K. Loh, E. Harris, D.J. Chou, Comparative study of heat pipes performances in different orientations, Annu. IEEE Semicond. Therm. Meas. Manag. Symp. (2005) 191–195, https://doi.org/10.1109/stherm.2005.1412178.
[56] M.S. Hosen, D. Karimi, T. Kalogiannis, A. Pirooz, J. Jaguemont, M. Berecibar, J. Van Mierlo, Electro-aging model development of nickel-manganese-cobalt lithium-ion technology validated with light and heavy-duty real-life profiles, J. Energy Storage 28 (2020) 101265, , https://doi.org/10.1016/J.EST.2020.101265.
[57] M. Sheikholeslami, D.D. Ganji, Heat transfer improvement in a double pipe heat exchanger by means of perforated turbulators, Energy Convers. Manag. 127 (2016) 112–123, https://doi.org/10.1016/J.ENCONMAN.2016.08.090.
[58] M. Sheikholeslami, D.D. Ganji, Heat transfer enhancement in an air to water heat exchanger with discontinuous helical turbulators; experimental and numerical studies, Energy 116 (2016) 341–352, https://doi.org/10.1016/J.ENERGY.2016.09.120.
[59] M.H.A. Elnaggar, M.Z. Abdullah, S. Raj, R. Munusamy, Experimental and numerical studies of finned L-shape heat pipe for notebook-PC cooling, IEEE Trans. Components, Packag. Manuf. Technol. 3 (2013) 978–988, https://doi.org/10.1109/TCPMT.2013.2245944.
[60] M. Soltani, G. Berckmans, J. Jaguemont, J. Ronsmans, S. Kakihara, O. Hegazy, J. Van Mierlo, N. Omar, Three dimensional thermal model development and validation for lithium-ion capacitor module including air-cooling system, Appl. Therm. Eng. 153 (2019) 264–274, https://doi.org/10.1016/j.applthermaleng.2019.03.023.
[61] M. Soltani, J. Ronsmans, J. Jaguemont, J. Van Mierlo, P. Van Den Bossche, N. Omar, A Three-dimensional thermal model for a commercial lithium-ion capacitor battery pack with non-uniform temperature distribution, Proc. IEEE Int. Conf. Ind. Technol. 2019-Febru. 2019, pp. 1126–1131, , https://doi.org/10.1109/ICIT.2019.8755081.
[62] J. Jaguemont, L. Boulon, Y. Dubé, Characterization and modeling of a hybrid-electric-vehicle lithium-ion battery pack at low temperatures, IEEE Trans. Veh. Technol. 65 (2016) 1–14, https://doi.org/10.1109/TVT.2015.2391053.
[63] L. Zhao, J. Wang, Y. Li, Q. Liu, W. Li, Experimental investigation of a lithium battery cooling system, Sustain (2019) 11, https://doi.org/10.3390/su11185020.
[64] M. Ghanbarpour, R. Khodabandeh, Entropy generation analysis of cylindrical heat pipe using nanofluid, Thermochim. Acta 610 (2015) 37–46, https://doi.org/10.1016/j.tca.2015.04.028.
[65] A. Pesaran, Battery thermal management in EVs and HEVs : issues and solutions, Adv. Automot. Batter. Conf, 2001, p. 10.
[66] S. Pesaran, A. Keyser, M. Burch, An Approach Des. Therm. Manag. Syst. Electr. Hybrid Veh. Batter. Packs, (1999) United States.
[67] M. Soltani, J. Ronsmans, S. Kakihara, J. Jaguemont, P.Van den Bossche, J. van Mierlo, N. Omar, Hybrid battery/lithium-ion capacitor energy storage system for a pure electric bus for an urban transportation application, Appl. Sci. (2018) 8, https://doi.org/10.3390/app8071176.
[68] S.J. Wang, A.S. Mujumdar, A comparative study of five low Reynolds number k-ε models for impingement heat transfer, Appl. Therm. Eng. 25 (2005) 31–44, https://doi.org/10.1016/j.applthermaleng.2004.06.001.
[69] P. Jagadeesh, K. Murali, Application of low-Re turbulence models for flow simulations past underwater vehicle hull forms, J. Nav. Archit. Mar. Eng. 2 (1970) 41–54, https://doi.org/10.3329/jname.v2i1.2029.
[70] C. Wang, G. Zhang, L. Meng, X. Li, W. Situ, Y. Lv, M. Rao, Liquid cooling based on thermal silica plate for battery thermal management system, Int. J. Energy Res. 41 (2017) 2468–2479.